Journal of Solid State Chemistry **149,** 308–313 (2000)
doi:10.1006/jssc.1999.8531, available online at http://www.idealibrary.com on IDEAL®

Crystal Structure and Polarized Raman Spectra of $Ca_6Sm_2Na_2(PO_4)_6F_2$

Mohamed Toumi,* Leila Smiri-Dogguy,* and Alain Bulou†

*Laboratoire de Chimie Inorganique et Structurale, Faculté des Sciences de Bizerte, 7021 Zarzouna, Tunisia; and †Laboratoire de Physique de l'Etat Condensé, UPRES-A CNRS 6087, Faculté des Sciences, Université du Maine, 72085 Le Mans Cédex 09, France

Received August 4, 1999; in revised form September 29, 1999; accepted October 11, 1999

The crystal structure of a new apatite $Ca_6Sm_2Na_2(PO_4)_6F_2$ has been determined using 842 independent reflections ($R = 0.059$, $R_w = 0.076$). The unit cell constants are $a = 9.3895(3)$ Å, $c = 6.8950(4)$ Å with $P6_3/m$ space group. The structure contains disordered cations in both the Ca(1) and the Ca(2) sites. The formula assigned to the compound is $[Ca_{1.57}Sm_{0.43}Na_2](1)[Ca_{4.43}Sm_{1.57}](2)(PO_4)_6F_2$. The Raman spectra have been studied and they are consistent with the proposed structure. A comparison with fluorapatite shows that most of the Raman lines of the new compound are significantly broad, which is attributed to the random distribution of three kinds of atoms on the cation sites. © 2000 Academic Press

Key Words: **apatite; X-ray determination of structure; Raman scattering.**

INTRODUCTION

Compounds of the apatite type have been widely studied since they can be used for various applications such as catalysts (1), ionic exchangers (2), and luminescent materials (3–5). The reference crystal is the calcium fluorapatite (FAp) $Ca_{10}(PO_4)_6F_2$ that crystallizes in the hexagonal system with the $P6_3/m$ space group (6). This structure is characterized by a unit cell containing six PO_4 tetrahedra on mirror planes at $z = 1/4$ and $z = 3/4$, both bonded to Ca^{2+} ions. These cations occupy two different crystallographic sites. Ca(1) is found, approximately midway between the mirror planes, in columns at $x = 1/3$, $y = 2/3$. Ca(2) is arranged in the mirror planes in triangles centered on the screw axis at $x = y = 0$. The two F^- ions sit on this screw axis.

The incorporation of foreign cations in the apatite structure is expected to give materials with different bulk properties. Unfortunately, it is usually not possible to *a priori* predict the distribution of rare-earth elements (REE) over the two nonequivalent crystallographic sites of apatite. In Nd-doped $Sr_{10}(VO_4)_6F_2$, neodymium substitutes into both Sr(1) and Sr(2) (7), but in $Sr_{10}(PO_4)_6F_2$ it substitutes only in the Sr(2) site. For Nd-doped FAp, the REE site preference also appears to depend on the substitution mechanism (8). If doping is performed with NdF_3, neodymium substitutes equally into both Ca(1) and Ca(2), but when Nd_2O_3 is used, it substitutes only in Ca(2). In $Ca_9Nd(PO_4)_5(SiO_4)F_{1.5}O_{0.25}$, the neodymium is distributed over both calcium sites, 17% in Ca(1) and 83% in Ca(2) (9). In $Ba_6La_2Na_2(PO_4)_6F_2$, ($P\bar{6}$ space group), La and Na occupy in a disordered way the column positions (Ca(1)), as well as the triangle positions (Ca(2)) (10). For $Ba_4Nd_3Na_3(PO_4)_6F_2$, $P\bar{3}$ space group, Nd and Na are ordered in the column sites (Ca(1)), but there is a disorder of the rest of these ions in the triangle position (Ca(2)). In $Na_2Eu_2Ca_6(PO_4)_6F_2$ (11), the Eu^{3+} ions are mainly located in the Ca(1) site (about 75%), and the Na^+ ions can only be located in the Ca(2) site.

In order to get a better understanding of these puzzling effects, we undertook a systematic study of the apatites containing REE. This paper is devoted to the case of a crystal based on samarium.

EXPERIMENTAL PROCEDURES

A. Preparation

Single crystals of $Ca_6Sm_2Na_2(PO_4)_6F_2$ (hereafter referred as CSNP) were obtained by solid-state reaction of $CaCO_3$, $(NH_4)_2HPO_4$, Sm_2O_3, and NaF in molar proportions (6:6:1:10). After grinding, the mixture was heated at 400°C for 4 h, then at 1200°C for 1 h, and finally gradually cooled (10°C/h) to room temperature. Small needle-shape crystals were separated from the flux by repeated washing in hot water.

B. Raman Spectrometry

The Raman spectra were recorded with a DILOR Z24 single-channel spectrometer. An argon laser (Coherent Innova 90.3) was used for the excitation: the 514.5 nm wavelength radiation was chosen since the possible luminescence lines from samarium are weak and out of the spectral range where the Raman signals appear. The spectral width (full width at half maximum) is less than 6 cm^{-1}, and the error on the line positions is less than 1 cm^{-1}. The

0022-4596/00 $35.00

measurements were done at room temperature under a microscope (in the back-scattering geometry) on micrometric samples fixed on a goniometric head and orientated in order to do polarization analysis; a X50 objective with a long working distance was chosen in order to ensure fairly good polarization conditions.

RESULTS AND DISCUSSION

A. Structure

1. Refinement of the structure. The X-ray diffraction intensities from a single crystal ($0.057 \times 0.049 \times 0.171$ mm^3) were collected using a Siemens AED2 four-circle diffractometer with graphite monochromated Mo$K\alpha$ radiation ($\lambda = 0.7107$ Å). The unit cell parameters were determined by a least-squares fit of 36 randomly located reflections. The total sphere of reflection with $1^\circ < 2\theta < 70^\circ$ was measured, and three standard reflections were monitored every hour. No absorption correction was applied ($R\mu < 2$).

The crystallographic characteristics and conditions for data collection are given in Table 1a. The structure refinements were performed with SHELXL-93 (12) programs. An equal distribution of Na and Sm into both Ca(1) and Ca(2) sites was assumed as a starting model. After refinement, one obtains 10.75% Sm, 39.25% Ca, and 50% Na in the Ca(1) site and 26.16% Sm and 73.84% Ca in the Ca(2) site. Hence, the structure of $Ca_6Sm_2Na_2(PO_4)_6F_2$ contains disordered cations in both the Ca(1) and the Ca(2) sites, so the formula assigned to the compound must be

$$[Ca_{1.57}Sm_{0.43}Na_2](1)[Ca_{4.43}Sm_{1.57}](2)(PO_4)_6F_2.$$

TABLE 1a
Crystallographic Characteristics and Measuring and Refinement Conditions of $Ca_6Sm_2Na_2(PO_4)_6F_2$

Crystal data	
Chemical formula	$Ca_6Sm_2Na_2(PO_4)_6F_2$
Crystal system	hexagonal
Space group	$P6_3/m$
Lattice constants (Å)	$a = 9.3895(3)$; $c = 6.8950(4)$
Data collection	
Diffractometer	AED2
Radiation	λ(Mo$K\alpha$) = 0.7107 Å
Scan mode	ω–2θ
Theta range (°)	1–70
Collected reflections	842
Independent reflections	826
Observed reflections	573 [$F_O > 4\sigma(F_O)$]
Refinement	
Parameters	45
$R = \sum \|\|F_O\| - \|F_C\|\| / \sum \|F_O\|$	0.0597 [0.026 for $F_O > 4\sigma(F_O)$]
$R_w = [\sum \|\|F_O\| - \|F_C\|\|^2 / \sum w\|F_O\|^2)]^{1/2}$	0.0763
$S = 1.03$	

TABLE 1b
Ionic Coordinates and Isotropic Thermal Parameters of $Ca_6Sm_2Na_2(PO_4)_6F_2$ Refined in the $P6_3/m$ Space Group

	Site	x	y	z	U_{eq}
M(1)[a]	4*f*	1/3	2/3	0.0005(1)	0.0110(2)
M(2)[a]	6*h*	0.24726(5)	0.01079(6)	1/4	0.0097(1)
F	2*a*	0	0	1/4	0.0179(9)
P	6*h*	0.3688(1)	0.3966(1)	1/4	0.0041(1)
O(1)	6*h*	0.4680(3)	0.5855(3)	1/4	0.0119(5)
O(2)	6*h*	0.4803(3)	0.3217(3)	1/4	0.0097(4)
O(3)	12*i*	0.2554(2)	0.3393(2)	0.0721(3)	0.0137(4)

[a] The occupancy at the Ca(1) site is 0.5 Na, 0.393(1) Ca, and 0.107(1) Sm; at the Ca(2) site it is 0.738(1) Ca and 0.262(1) Sm.

The final Fourier-difference map ranges from $+0.91$ e.Å^{-3} to -0.75 e.Å^{-3}.

The atomic positions, selected bond lengths, and angles are reported in Tables 1b and 1c, respectively.

2. Discussion. Our refined results indicate that the Sm^{3+} ions are mainly located in the Ca(2) site (about 78.5%), while the Na^+ ions sit only in the Ca(1) site. The total substitution of Na^+ in the Ca(1) site and the preference of Sm^{3+} for the Ca(2) can be explained by the following qualitative considerations:

— The electrostatic repulsion energy can be lowered by setting in the Ca(1) site (column), where the cation– cation distance is short (3.447 Å), the Na^+ ions with low charge, leaving the triangle sites (Ca(2)) with longer interionic distances (3.936 Å) for the highly charged Sm^{3+}.

— The Ca(2) sites are surrounded by four PO_4 groups, and the Ca(1) sites are surrounded by six. So, the Sm^{3+}–P^{5+} repulsion energy is minimized by placing the fewest Sm^{3+} ions in the Ca(1) sites.

These considerations presumably drive the strong preference of Sm^{3+} for the Ca(2) site, but this influence is limited by the bond valence requirements of the F^- anion. This is why the substitution of Sm^{3+} in the Ca(1) site is not total.

TABLE 1c
Bond Lengths (Å) and Selected Angles (°) of $Ca_6Sm_2Na_2(PO_4)_6F_2$

M(1)–O(2) × 3	2.422(2)	P–O(2)	1.525(3)
–O(1) × 3	2.470(2)	P–O(3) × 2	1.535(2)
–O(3) × 3	2.824(2)	P–O(1)	1.537(3)
M(2)–O(3) × 2	2.358(2)		
–O(1)	2.410(3)	O(2)–P–O(3) × 2	110.7(1)
–O(3) × 2	2.504(2)	O(1)–P–O(3) × 2	108.5(1)
–O(2)	2.632(3)	O(1)–P–O(2)	111.8(1)
–F	2.273(1)	O(3)–P–O(3)	106.1(1)

Concerning the tetrahedra, the average P–O distance (1.533 Å) is similar to the value observed in FAp (1.535 Å) (13). On the other hand, the distortions are significantly larger: this can be quantitatively characterized by the variance σ defined by

$$\sigma^2 = 1/6 \sum(\theta_i - 109.47)^2,$$

where θ_i represents each of the O–P–O bond angles and 109.47° is the O–P–O bond angle in the ideal PO_4 tetrahedron. So, one obtains $\sigma^2 = 3.69$ in the CSNP instead of 2.89 in the FAp.

Concerning the cations, like in $Na_2Eu_2Ca_6(PO_4)_6F_2$ (11), the average (Na1,Ca1,Sm1)–O distance (2.572(2) Å) and (Ca2,Sm2)–O distance (2.461(2) Å) are slightly larger than the average values observed in FAp (2.56(20) Å and 2.44(13) Å (13)). The (Sm2,Ca2)–F distance, 2.273 Å, is larger than the (Eu2,Ca2)–F distance, 2.265 Å, in $Na_2Eu_2Ca_6(PO_4)_6F_2$ (11). The variation could be explained by considering the size (14) of cations (Sm^{3+}/Eu^{3+}).

The larger distortion of the PO_4 tetrahedra and the distribution of the interionic M–O distances are obviously due to the distortion of the coordination polyhedra resulting from the disorder on the calcium sites. As a matter of fact, the local coordination of the ions occupying the column position differs significantly; Na^+ usually requires six-coordination while Ca^{2+} and Sm^{3+} are more commonly found with nine.

B. Vibrational Spectra Analysis

1. Group theory and polarization. Factor group analysis (15) of the hexagonal fluorapatite structure ($P6_3/m$, $Z = 2$) shows that the normal modes of vibration can be classified among the irreducible representations of C_{6h} as

$$\Gamma_M = 12A_g + 8E_{1g} + 13E_{2g} + 9A_u + 12B_u + 9B_g + 13E_{1u} + 8E_{2u},$$

where the internal mode contribution of the PO_4 groups is

$$\Gamma_{PO_4} = 6A_g + 3E_{1g} + 6E_{2g} + 3A_u + 6B_u + 3B_g + 6E_{1u} + 3E_{2u}.$$

The optical modes are obtained after taking off the acoustic modes with symmetries

$$\Gamma_{acoustic} = A_u + E_{1u}.$$

The A_g, E_{1g}, and E_{2g} symmetry modes are Raman active, and the corresponding polarization tensors are given in Table 2. So, 33 lines are expected in the Raman spectra. The contributions of the different ions and the [PO_4] tetrahedron to the Raman-active vibrations are distributed as follows:

TABLE 2
Polarizability Tensors Corresponding to the Raman-Active Modes of $Ca_6Sm_2Na_2(PO_4)_6F_2$

A_g			E_{1g}			E_{2g}		
a	·	·	·	·	d	e	f	·
·	a	·	·	·	c	f	−e	·
·	·	b	d	c	·	·	·	·

$$\Gamma_F = E_{2g}$$

$$\Gamma_{[CaNaSm](1)} = A_g + E_{1g} + E_{2g}$$

$$\Gamma_{[CaSm](2)} = 2A_g + E_{1g} + 2E_{2g}$$

$$\Gamma_{PO_4} = 6A_g + 3E_{1g} + 6E_{2g} \text{ (internal modes)}$$
$$3A_g + 3E_{1g} + 3E_{2g} \text{ (external modes).}$$

This shows that all the ions are potentially involved in the E_{2g} modes and that the fluorine ions do not participate in the vibrations with A_g and E_{1g} symmetries. Concerning the internal modes of the PO_4, they derive from the modes of the free tetrahedron with symmetries A_1 (referred to as v_1), E (v_2), and F_2 (v_3 and v_4) of the corresponding T_d point group. In the $P6_3/m$ space group they lead to the symmetries given in Table 3 (limited to the Raman-active modes). It appears that 2, 3, and 5 lines are expected for each of these symmetries, respectively.

2. Results and discussion. Polarized Raman spectra were recorded for different orientations of the crystal (the crystals looking like needles parallel to the [001] axis and exhibiting clear growth faces). The A_g, E_{1g}, and E_{2g} modes were obtained in the $X(ZZ)\bar{X}$, $X(ZY)\bar{X}$, and $Z(XY)\bar{Z}$ geometries, respectively (Table 2); the $X(YY)\bar{X}$ geometry gives both the A_g and the E_{2g} modes; the spectra are shown in Fig. 1. Several high-resolution spectra were also recorded in the vicinity of 960 cm^{-1} to look for the possible existence of

TABLE 3
Raman Line Symmetries in the $P6_3/m$ Space Group Corresponding to the Modes of the Free PO_4 Tetrahedron

Free ion (T_d point group)	FAp, CSNP ($P6_3/m$ space group)
A_1	$A_g + E_{2g}$
E	$A_g + E_{1g} + E_{2g}$
F_2	$2A_g + E_{1g} + 2E_{2g}$

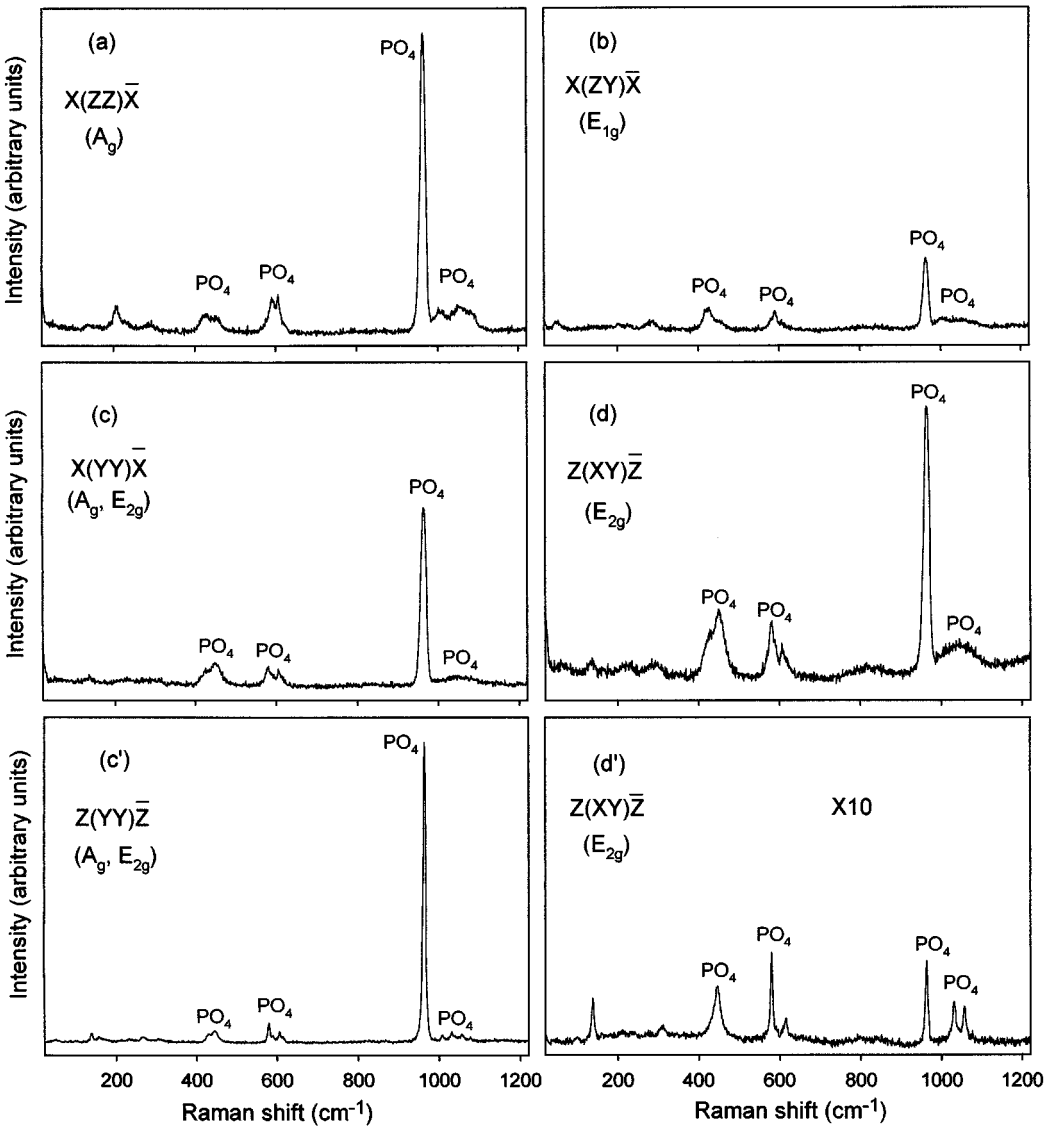

FIG. 1. Raman spectra of $Ca_6Sm_2Na_2(PO_4)_6F_2$ (a–d) and $Ca_{10}(PO_4)_6F_2$ (c′, d′) collected in various geometries. The geometries and the corresponding mode symmetries are given in each diagram. It can be noted that the intensities of the spectra of Fig. d′ have been expanded by 10. The lines mainly involving PO_4 internal vibrations are indicated on the diagrams.

several components. Moreover, to elucidate the main characteristics of the spectra, it is useful to do a comparison with the isomorphic fluorapatite $Ca_{10}(PO_4)_6F_2$. So, Raman spectra of this compound were collected under the same experimental conditions, and some of them are drawn in Fig. 1.

It appears that the spectra of CSNP and FAp are very close, mainly dominated by the internal modes of the PO_4. They show a very intense line corresponding to the ν_1 stretching mode (located at 938 cm^{-1} for the free ion (16)) and weak intensity bands corresponding to the ν_2 mode (at 420 cm^{-1} for the free ion (16)) and to the ν_3 and ν_4 modes (at 1017 and 567 cm^{-1}, respectively, for the free ion (16)). They are in the same frequency range in both compounds. On the other hand, while the lines are narrow and well defined in FAp, in CSNP one observes much broader signals (Fig. 1): for example, the A_g signal corresponding to the nondegenerate ν_1 mode is less than 1 cm^{-1} FWHM in the former but about 10 cm^{-1} in the latter (note, however, that no fine structure was observed in the high-resolution spectra, as predicted from Table 3, which supports the high symmetry $P6_3/m$ space group); the modes arising from ν_3 are even almost unresolved. These features can be attributed to the fact that the cationic sites (M(1) and M(2)) are randomly occupied by different ions (Ca^{2+}, Na^+, Sm^{3+}), so the different PO_4 experience different electric fields. The average

frequency remains, however, close to the usual value since the average charge remains the same in both compounds. The wavenumbers of the various lines associated with PO_4 vibrations are given in Table 4a. The attribution is done with respect to the FAp attribution taken from (17) since this work results from an analysis performed on a large single crystal (the present measurements, being realized under a microscope, cannot ensure such strict polarization conditions due to the large numerical aperture; it must be pointed out, however, that our results on FAp disagree with those of Ref. (17) for two A_g modes since we unambiguously found 1006 and 430 cm^{-1} instead of 1053 and 454 cm^{-1}). In CSNP it also appears that the selection rules are not strictly observed: in particular, a significant signal is seen in the $X(ZY)\bar{X}$ geometry in the frequency range of the stretching mode of PO_4, while, as indicated in Table 3, it should not be active; a similar remark applies to the ν_2 mode in the XY geometry, where a single line is expected, which indeed is clear in FAp (compare Figs. 1d and 1d′). These relaxations of the selection rules can be imputed to the lost of the translational periodicity resulting from the chemical disorder on the M(1) and M(2) sites. Before concluding, it is worth noting too that the E_{1g} line deriving from ν_4, reported in Ref. (17), was not observed in our investigation of FAp but is clearly seen in CSNP (Table 4a). Such a feature could be explained by the fact that this mode, presumably giving a weak Raman signal, belongs to a quasi-flat phonon branch (which is physically realistic for internal modes): the significant intensity observed in CSNP can again be a consequence of the breaking of the selection rules induced by disorder.

TABLE 4a

Experimental Wavenumbers (in cm^{-1}) of the PO_4^{3-} Tetrahedra Vibrations in $Ca_6Sm_2Na_2(PO_4)_6F_2$ (CSNP) and Fluorapatite (FAp)

After (17)		Our results		
Mode	FAp	FAp	CSNP	Attribution
A_g	1081	1078	≈ 1086	ν_3
E_{2g}	1059	1057	≈ 1052	
A_g	1053	1006	≈ 1005	
E_{1g}	1043			
E_{2g}	1033	1031		
A_g	965	963	965	ν_1
E_{2g}	947		955	
E_{2g}	616	615	617	ν_4
A_g	605	606	607	
E_{1g}	593		590	
A_g	590	591	593	
E_{2g}	580	580	580	
A_g	454	430	426	ν_2
E_{2g}	444	446	449	
E_{1g}	430			

TABLE 4b

The Translational–Orientational Vibration Wavenumbers (in cm^{-1}) of the Crystal Lattice of $Ca_6Sm_2Na_2(PO_4)_6F_2$ (CSNP) and Fluorapatite (FAp)

After (17)	Our results	
Symmetry	FAp	FAp	CSNP
E_{2g}	100		61
E_{1g}	104	98	53
E_{2g}	138	138	136
E_{1g}	140		
A_g	160		161
E_{2g}	166		
E_{1g}	182		
A_g	210		207
A_g	232	234	232
E_{1g}	234		204
E_{2g}	236		
E_{2g}	273		
A_g	278	266	
E_{1g}	290		288
A_g	297		291
E_{2g}	311	310	311

The external modes are found at lower frequencies, and again the bands are also usually broader than in FAp. The wavenumbers of the main identified bands are reported in Table 4b. The most interesting feature is the existence of a few lines with much weaker frequencies than in FAp. This can be attributed to the presence of much heavier ions. Actually, with regard to the huge mass of samarium with respect to the other components, several vibrations are presumably weakly coupled and some modes can involve this ion alone. This is probably the case for the two modes in the vicinity of 60 cm^{-1} since, with regard to the mass effect, they would correspond a vibration in the vicinity of 100 cm^{-1} in FAp, where lines are indeed observed. The fact that these modes appear with significant intensities (Fig. 1b) corroborates such an assumption with regard to the polarizability of the rare earth.

Finally, a broad signal is observed in the vicinity of 800 cm^{-1} in the E_{1g} and mostly E_{2g} geometries (Fig. 1d). This feature is actually also observed in the FAp (Fig. 1d′).

Before we conclude, it must be pointed out that the total number of experimentally observed lines remains smaller than the expected one, so the results of the spectroscopic study support the conclusions of the structural study.

CONCLUSION

In conclusion, the structure of the new compound $Ca_6Sm_2Na_2(PO_4)_6F_2$ has been determined, and it appears

that Ca, Sm, and Na are distributed over two sites (like in fluorapatite) but in different amounts. So, the substitution of 4 Ca by (2 Na + 2 Sm) does not cause significant changes in the structure. However, the tetrahedra are much more distorted. The numbers of internal modes of PO_4^{3-} and external modes observed in the Raman spectra are consistent with those predicted according to the proposed space group. The most striking difference from the fluorapatite is the significant broadenings of the lines, which can be explained as a consequence of the random distribution, over the cation sites, of three atoms (Ca, Na, Sm) very different in their charges and in their masses. Moreover, with respect to the fluorapatite, two modes undergo a large shift toward low frequency, which suggests vibrations mainly involving samarium displacements. So, the present work also contributes to the general analysis of the vibrational spectra of apatites.

REFERENCES

1. H. Monma, *J. Catal.* **75,** 200 (1982).
2. T. Suzuki, *Gypsum Lime* **204,** 314 (1986).
3. K. H. Butler, "Fluorescent Lamp Phosphors." Pennsylvania State University Press, University Park, PA, 1980.
4. G. Blasse, *Mater. Chem. Phys.* **16,** 201 (1987).
5. M. Tachihante, D. Zanbon, and J. C. Cousseins, *Eur. J. Solid State Inorg. Chem.* **33,** 713 (1996).
6. S. Naray-Szabo, *Z. Kristallogr.* **75,** 323 (1930).
7. B. L. Corker, B. H. T. Chai, J. Nicholls, and G. B. Loutts, *Acta Crystallogr.* **C51,** 549–551 (1995).
8. P. E. Machie and R. A. Young, *J. Appl. Crystallogr.* **6,** 26 (1973).
9. L. Boyer, J. M. Savariault, J. Carpena, and J. L. Lacout, *Acta Crystallogr.* **C54,** 1057–1059 (1998).
10. M. Mathew, I. Mayer, B. Dickens, and L. W. Schroeder, *J. Solid State Chem.* **28,** 79 (1979).
11. I. Mayer and S. Cohen, *J. Solid State Chem.* **48,** 17–20 (1983).
12. G. M. Sheldrick, Program for the Refinement of Crystal Structures, University of Göttingen, Germany, 1993.
13. K. Sudarsanan, P. E. Mackie, and R. A. Young, *Mater. Res. Bull.* **7,** 1331–1338 (1972).
14. R. D. Shannon, *Acta Crystallogr. A* **32,** 751–767 (1976).
15. W. G. Fateley, F. R. Dollish, N. T. Mc Devitt, and F. F. Bentley, "Infrared and Raman Selection Rules for Molecular and Lattice Vibrations: The Correlation Method." Wiley–Interscience, New York, 1972.
16. K. Nakamoto, "Infrared Spectra of Inorganic and Coordination Compounds." Wiley–Interscience, New York, 1986.
17. Yu. K. Voron'ko, A. V. Gorbachev, A. A. Zverev, A. A. Sobol', N. N. Morozov, E. N. Murav'ev, Sh. A. Niyazov, and V. P. Orlovskii, *Neorganich. Mater.* **28,** 582 (1992).